High-temperature spin dynamics of a cubic ferromagnet Pd_2MnSn

M. Kohgi, Y. Endoh, and Y. Ishikawa*
Physics Department, Tohoku University, Sendai 980 Japan

H. Yoshizawa† and G. Shirane
Physics Department, Brookhaven National Laboratory, Upton, New York 11973
(Received 27 January 1986)

The paramagnetic scattering function $S(q,\omega)$ of the metallic ferromagnet Pd_2MnSn has been investigated up to $4T_C$ over a wide q range along the [100], [011], and [111] directions by means of both polarized and unpolarized neutron scattering techniques. The temperature and q dependence of the static response, $k_BT\chi(q)$, is explained rather well by the Heisenberg model with long-range interactions, although there are nontrivial deviations from the theory. The features of the dynamical response are summarized as follows: (i) The scattering function has a simple one-peak form centered at $\hbar\omega=0$ in the whole q range at $1.5T_C$ and $4T_C$. (ii) The linewidths of the function near zone boundaries agree well with the calculations based on the three-pole approximation of the Heisenberg model. (iii) The linewidths near $q=0$ show the anomalously large temperature dependence, and have no q^2 dependence at $4T_C$. These facts point to the importance of the nonadiabatic effects of the conduction electrons at high temperatures, even though the Heisenberg-type interactions between localized spins play the major role on the spin dynamics in this system.

I. INTRODUCTION

The neutron scattering study of the spin dynamics of the $3d$ metallic ferromagnets above T_C is one of the most challenging subjects in solid-state physics. There is no satisfactory theoretical understanding, nor is there even an agreement on the interpretation of the experimental results on the itinerant ferromagnets Fe and Ni.[1-7] The point of controversy is whether a spin-wave-like mode with fairly small wave vectors exists above T_C in Fe and Ni. At this stage, it is very important to understand fully the spin fluctuations of the typical localized system at high temperatures. This, in turn, may be helpful for an understanding of the more difficult cases of itinerant systems.

The intermetallic compound Pd_2MnSn is a typical ferromagnetic Heusler alloy with the Curie temperature $T_C=190$ K. The manganese sublattice forms a fcc structure with the lattice parameter $a=6.38$ Å. The susceptibility obeys the Curie-Weiss law with an effective moment of $p_{\text{eff}}=4.7\mu_B$ per manganese atom and the atomic moment estimated from this value is in agreement with the observed saturation moment.[8] The neutron scattering measurements below T_C performed by Noda and Ishikawa[9] show that the spin-wave dispersion relations and their temperature dependence are described well by the Heisenberg model if more than six long-range exchange-interaction parameters are taken into account. The exchange parameters determined at 50 K are listed in Table I for the sixth- and eighth-nearest-neighbor cases.[9] The calculated paramagnetic Curie temperatures using these parameters are in good agreement with the observed value of $\Theta_p=201\pm3$ K. Ziebeck *et al.*[10] observed the complete paramagnetic neutron scattering at $4T_C$ by using a powder sample and without energy analysis. These experimental results clearly show that Pd_2MnSn can be regarded as a typical localized spin system.

Recently Shirane *et al.*[11] performed a detailed study of paramagnetic scattering from Pd_2MnSn near T_C (up to $1.5T_C$) by using a single-crystal sample. It was found that the observed scattering function $S(Q,\omega)$ can be described by a simple double Lorentzian form,

$$S(Q,\omega)=S_0\frac{\kappa_1^2}{\kappa_1^2+q^2}\frac{\Gamma}{\Gamma^2+\omega^2} \tag{1}$$

over a wide q range. No propagating mode was observed above T_C, which is in contrast to the case of the insulating ferromagnet EuO,[12,13] where a spin-wave-like mode was observed near the zone boundary. It was also revealed that the constant-E scans above T_C give an intensity ridge which has a magnonlike dispersion and is almost temperature independent up to $1.5T_C$. The position of the constant-E ridge at T_C is very close to those of the itinerant ferromagnetics Fe (Refs. 1 and 3) and Ni (Refs. 2 and 4) when the momentum and energy are scaled by the inverse plane distance d^* and diffusion constant A ($\Gamma=Aq^{5/2}$), respectively. This result is well explained by the dynamical scaling theory.

This work raised a new question about the differences in the spin dynamics between Pd_2MnSn and the insulating ferromagnets EuO and EuS. The best way to approach this problem is to study the spin dynamics of these materials at higher temperatures, since the differences in the spin dynamics in the different interaction systems are considered to appear more clearly at high temperatures. This may also be helpful for the study of the spin dynamics of itinerant systems. We have therefore extended the study of the paramagnetic scattering from Pd_2MnSn up to $4T_C$ in a wide momentum and energy space by means of

TABLE I. Exchange parameters (meV) of Pd_2MnSn (Ref. 9).

J_1	J_2	J_3	J_4	J_5	J_6	J_7	J_8	Θ_p (K)	D (meV Å^2)
0.195	0.130	0.066	−0.133	0.042	−0.057	0.011	−0.017	205.0	106.2
0.216	0.111	0.066	−0.123	0.046	−0.039			209.2	91.5

polarized and unpolarized neutron scattering techniques. We describe below the results of the measurements, and compare them with the existing theories[14–16] based on the Heisenberg model as well as with the experimental results on the insulating ferromagnets EuO (Refs. 12, 13, and 17) and EuS.[18]

II. EXPERIMENTAL DETAILS

The neutron scattering measurements were carried out on triple-axis spectrometers at the Brookhaven High Flux Beam Reactor. The single crystal used in the experiments was identical to that used in the previous work by Shirane *et al.*;[11] the volume is about 3 cm^3 and the mosaic spread is 0.8°. It was mounted in a furnace or in a cryostat with the [011] axis vertical. The paramagnetic scattering was measured along the three principal axes [100], [011], and [111] around the (1,1,1) reciprocal-lattice point mainly at 294 K ($1.5T_C$) and 773 K ($4T_C$) by using polarized and unpolarized beam techniques. For the polarized beam setup, we used copper Heusler (111) crystals as monochromator and analyzer with the fixed final energy of 32 meV. The horizontal and vertical collimations were 40′-80′-80′-80′ and 50′-110′-150′-240′, respectively. The energy resolution of this configuration was about 2.5 meV [full width at half maximum (FWHM)] at $\hbar\omega=0$. The difference of the intensity measured with a horizontal field (HF) and a vertical field (VF), with the flipper on, was employed to get the reliable paramagnetic scattering function.[10]

A high-resolution unpolarized beam setup was also used to measure the paramagnetic scattering near the zone center where the half-widths of the scattering function are less than 2 meV. Both monochromator and analyzer in this case were pyrolitic graphite (002) crystals operating with the fixed incident energy of 14.7 meV. The horizontal collimations were 20′-20′-20′-20′ and the vertical collimations were nearly the same as the polarized neutron experiments. A pyrolitic graphite filter was used to eliminate higher-order contamination of the beam.

In order to put the paramagnetic cross section on an absolute scale, we utilized the intensities of the spin-wave scattering measured at 80 K for the same spectrometer configuration. It is not appropriate to use phonon intensities[3] for our case because there is no reliable data for the phonon cross section of Pd_2MnSn.

III. THEORETICAL EXPRESSIONS

The inelastic scattering cross section for unpolarized neutrons by a magnetic system of N-localized spins is given by[19]

$$\frac{d^2\sigma}{d\Omega\, d\omega}=N\gamma_0^2\frac{k_f}{k_i}\left|\tfrac{1}{2}gf(Q)\right|^2 e^{-2W}S(q,\omega)\ , \tag{2}$$

where $\gamma_0^2=0.291$ b/sr, k_f and k_i are the wave vectors of the final and incident neutrons, g is the gyromagnetic ratio, and $f(Q)$ is the form factor. The scattering function $S(q,\omega)$ above T_C for unpolarized neutrons is expressed as

$$S(q,\omega)=2k_BT\chi(q)\frac{1}{(g\mu_B)^2}\frac{\hbar\omega\beta}{1-\exp(-\hbar\omega\beta)}F(q,\omega)\ . \tag{3}$$

Here, $\chi(q)$ and $F(q,\omega)$ are the wavelength-dependent susceptibility and the spectral shape function, respectively, and $\beta=1/k_BT$.

The wavelength-dependent susceptibility of the Heisenberg systems is evaluated by the spherical approximation as[15]

$$\chi(q)=\frac{1}{2[J(0)-J(q)]/(g\mu_B)^2+1/\chi}\ , \tag{4}$$

where $J(q)$ is the Fourier transform of the exchange constant J_{ij} between spins at site i and j and χ is the uniform field susceptibility. This expression is also valid in the molecular field approximation.[19]

The spectral shape function $F(q,\omega)$ above T_C has been calculated by several authors using different approximations.[14–16,20] Their results are different in detail but are similar in describing the overall features of $F(q,\omega)$. We mainly analyzed our data by using the result of the three-pole approximation[15] because of its simple analytical expressions as well as its successes in interpreting the observed spectral shapes for a number of Heisenberg systems: $RbMnF_3$,[15] EuO,[13,21] and EuS.[18,21] In this case, $F(q,\omega)$ is approximated by

$$F(q,\omega)=\frac{1}{\pi}\frac{\tau\delta_1\delta_2}{[\omega\tau(\omega^2-\delta_1-\delta_2)]^2+(\omega^2-\delta_1^2)^2}\ , \tag{5}$$

where δ_1 and δ_2 are the correlation functions and τ is the termination function. These are expressed as

$$\delta_1=\langle\omega^2\rangle,\quad \delta_2=\langle(\omega^2-\langle\omega^2\rangle)^2\rangle\ ,$$

and

$$\tau=(\pi\delta_2/2)^{-1/2}\ , \tag{6}$$

where $\langle\omega^2\rangle$ and $\langle\omega^4\rangle$ are the second and fourth moments of $F(q,\omega)$. At $T=\infty$, the moments can be easily calculated as[22]

$$\langle\omega^2\rangle=\tfrac{8}{3}S(S+1)\sum_l J_l^2[1-\cos(\mathbf{q}\cdot\mathbf{l})]\ ,$$

$$\langle\omega^4\rangle=32\left[\frac{S(S+1)}{3}\right]^2\left[-\sum_{\mathbf{R}}J_{\mathbf{R}}^4[1-\cos(\mathbf{q}\cdot\mathbf{R})]\left[4+\frac{3}{2S(S+1)}\right]+\left[\sum_{\mathbf{A}}J_{\mathbf{A}}^2[1-\cos(\mathbf{q}\cdot\mathbf{A})]\right]\left[\sum_{\mathbf{R}}J_{\mathbf{R}}^2[7-3\cos(\mathbf{q}\cdot\mathbf{R})]\right]\right.$$
$$\left.-2\sum_{\mathbf{A}}\sum_{\mathbf{R}}J_{\mathbf{A}}J_{\mathbf{R}}J_{\mathbf{A}-\mathbf{R}}(1-e^{i\mathbf{q}\cdot\mathbf{A}})[J_{\mathbf{R}}e^{-i\mathbf{q}\cdot\mathbf{A}}+J_{\mathbf{A}-\mathbf{R}}(1-e^{-i\mathbf{q}\cdot\mathbf{A}})]\right]\ . \tag{7}$$

IV. SPECTRAL SHAPE

Figure 1 shows the observed spectra at $\mathbf{Q}=(1.08,1.08,1.08)$ at (a) $1.7T_C$ and (b) $4T_C$, where the unpolarized neutron setup was used. Each component of the $\mathbf{Q}$ vector is measured in units of $2\pi/a$. Solid lines in the figure are the results of the least-squares fitting of the Lorentzian form of $F(q,\omega)$ convoluted with the resolution function to the data. In the fitting procedure, a constant background is assumed, and a few data points which are thought to be strongly contaminated by phonon and incoherent elastic scattering are eliminated. As seen in this figure, the observed spectra for this small momentum transfer are well described by the Lorentzian form of $F(q,\omega)$, although the counting statistics become poor at $4T_C$. Note particularly that the linewidth at $4T_C$ is significantly larger than that at $1.7T_C$.

Figures 2 and 3 show the observed spectra obtained by using polarized neutrons at $\mathbf{Q}=(1.25,1.25,1.25)$ and (1.4,1.4,1.4), respectively, at (a) $1.5T_C$ and (b) $4T_C$. No spin-wave-like peak is observed at either temperature within our experimental resolution and counting statistics. This is in agreement with the previous work,[11] but in contrast with the cases of EuO (Refs. 12 and 13) and EuS.[18] Solid and dashed lines in Figs. 2 and 3 show the results of the Lorentzian and Gaussian fitting, respectively. Below about $\hbar\omega=10$ meV it is not clear which function gives a better fit, but for $\hbar\omega\gtrsim 10$ meV it can be seen that the fit is better for the Lorentzian case. Figure 4(a) shows the intensity contour map of the resolution corrected scattering function $S(q,\omega)$ at $4T_C$ along the [111] direction for the case of the Lorentzian fit.

In order to compare the present results with the theory based on the Heisenberg model, we calculated the spectral shape function of Pd_2MnSn based on the three-pole approximation at $T=\infty$ [TPA, Eqs. (5)—(7)] with the exchange parameters up to the sixth-nearest neighbor listed in Table I. The data at $4T_C$ are compared with the calculation. Since the second and fourth moments of $F(q,\omega)$ at $T=\infty$ overestimate those at a finite temperature T by $\sim T_C J(q)/TJ(0)$ or less in fraction to order $1/k_BT$,[19] about 10% ambiguity of linewidth should be allowed for the comparison. Figure 5 shows the calculated $F(q,\omega)$

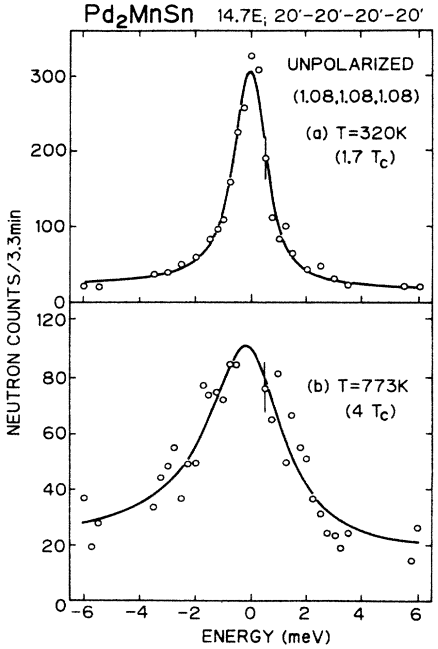

FIG. 1. Observed spectra at $\mathbf{Q}=(1.08,1.08,1.08)$ at (a) $1.7T_C$ and (b) $4T_C$. Solid lines are the curves fit to the data by employing the Lorentzian as the spectral shape function.

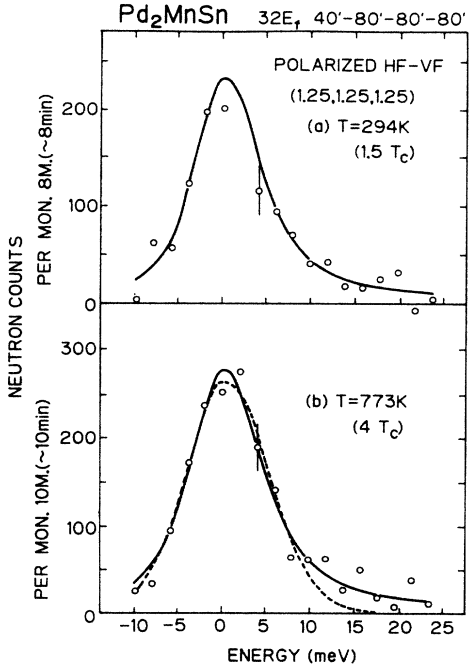

FIG. 2. Observed spectra at $\mathbf{Q}=(1.25,1.25,1.25)$ at (a) $1.5T_C$ and (b) $4T_C$. Monitor counts (MON) of 8 million correspond to approximately 8 min of counting time. Solid and dashed lines are the curves fit to the data by employing the Lorentzian and Gaussian, respectively, as the spectral shape function.

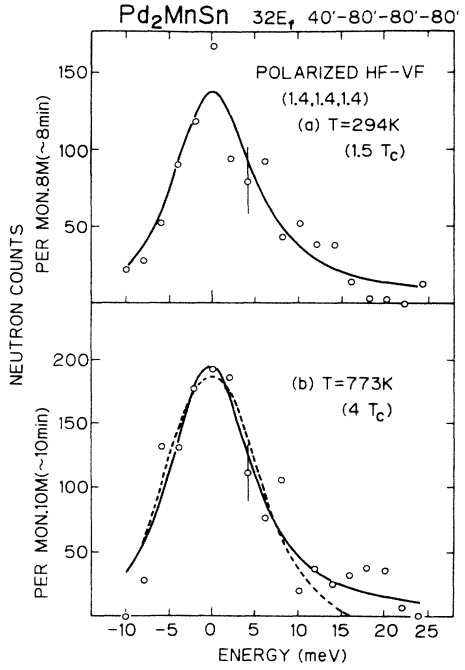

FIG. 3. Observed spectra at $\mathbf{Q}=(1.4,1.4,1.4)$ at (a) $1.5T_C$ and (b) $4T_C$. Solid and dashed lines are the curves fit to the data by employing the Lorentzian and Gaussian, respectively, as the spectral shape function.

along the [111] direction. It is also shown in the form of the contour map in Fig. 4(b). For the ζ value below about 0.1, the calculated spectral shape is very close to the Lorentzian. On the other hand, it shows a small shoulder at about $\hbar\omega=5$ meV for $\zeta\gtrsim 0.2$ and becomes almost independent of ζ for $\zeta\gtrsim 0.3$. Nearly the same spectral shapes are obtained along the [100] and [011] directions. This differs from the case of the short-range interaction Heisenberg systems EuO and EuS, where the TPA (Refs. 15 and 21) as well as the other approximations[14,16,20] gives more distinct peaks at nonzero energy transfer for the $\mathbf{q}$ vector near the zone boundaries. Therefore, it is concluded that the long-range interaction suppresses considerably such spin-wave-like modes for large $\mathbf{q}$ vectors.

In Fig. 6 a comparison of the observed and the theoretical spectra at $\mathbf{Q}=(1.4,1.4,1.4)$ is shown. The dashed line in the figure is the theoretical $F(q,\omega)$ without resolution convolution, and the solid line shows the resolution convoluted theoretical spectrum which should be compared with the observation (open circles). The dashed-dotted line is the result of the Lorentzian fit to the data. It is noted that the resolution effect smooths out completely the shoulder of the calculated spectral shape function, and that the resolution convoluted theoretical spectrum is very close to the result of the Gaussian fit to the observed data [see Fig. 3(b)]. Therefore, it is concluded that the Heisenberg model (TPA) can reproduce well the observed spectra for the large q values ($\zeta\gtrsim 0.2$) within our experimental accuracy, if we disregard the long tails observed for $\hbar\omega\gtrsim 10$ meV. This feature is also seen in the overall resemblance of the observed and calculated contour maps of $F(q,\omega)$ shown in Figs. 4(a) and 4(b). For the small q values ($\zeta\lesssim 0.2$), however, the linewidths at $4T_C$ are much larger than the theoretical values. This point will be discussed in the later sections.

V. WAVELENGTH-DEPENDENT SUSCEPTIBILITY

The wavelength-dependent susceptibilities $\chi(q)$ were deduced from the least-squares-fitting procedures to the data by assuming the spectral shape function to be a Lorentzian. For the data at $4T_C$, $\chi(q)$ is weakly q dependent and was assumed to be constant within the resolution ellipsoid. The value of $\chi(q)$ was determined from the scaling parameter in the fitting function. For the data at $1.5T_C$, on the other hand, we assumed as $\chi(q)=C(q)/(q^2+\kappa_1^2)$ in order to minimize the deforma-

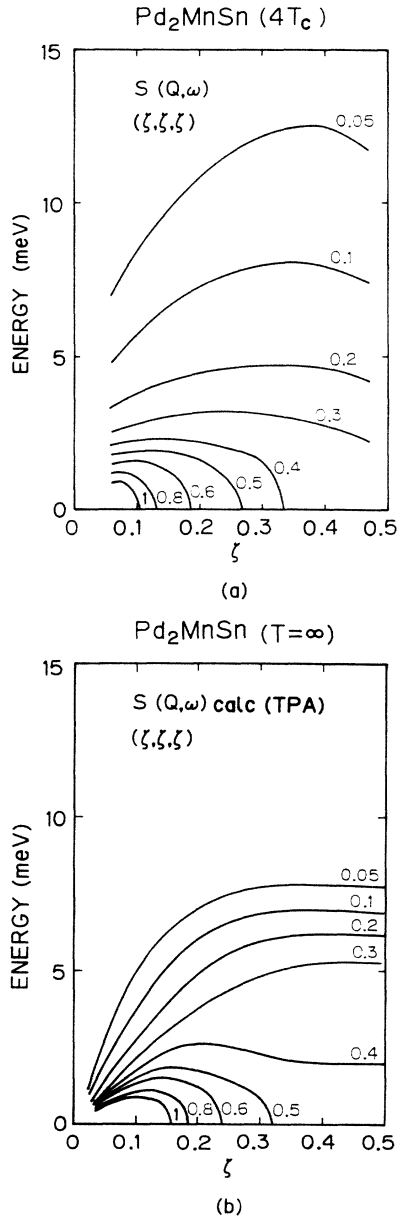

FIG. 4. (a) Contour map of the resolution corrected scattering function of Pd_2MnSn at $4T_C$ along the [111] direction. Lorentzian is assumed as the spectral shape function. (b) Contour map of the calculated scattering function for the Pd_2MnSn along the [111] direction by the three-pole approximation at $T=\infty$.

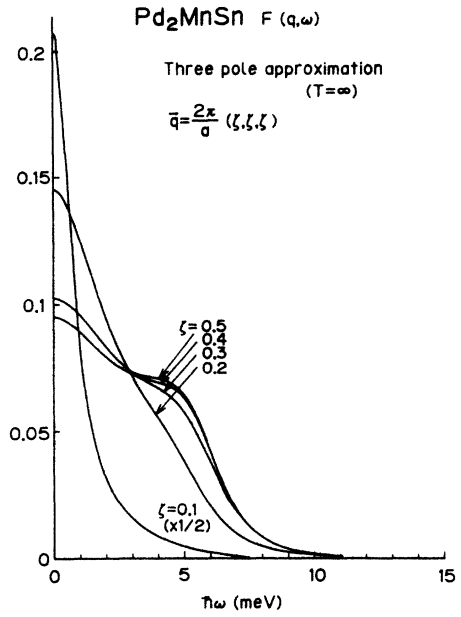

FIG. 5. Theoretical spectral shape functions along [111] calculated by the three-pole approximation at $T=\infty$.

tion by the resolution effect since the q dependence of $\chi(q)$ is very strong at this temperature. Here, $C(q)$, which is the correction factor to the simple Lorentzian for the susceptibility, was assumed to be constant within the resolution ellipsoid and left as the free parameter in the fitting procedures. κ_1 was taken to be 0.22 Å^{-1}, which is the inverse correlation length measured at $1.5T_C$.[11]

Figure 7(a) shows the wavelength-dependent susceptibilities obtained at $1.5T_C$ and $4T_C$ along the [111] direction in the form of $3k_BT\chi(q)$, which is equal to the energy integrated paramagnetic scattering $M^2(q)$ in the high-temperature limit ($\hbar\omega \ll k_BT$) and to $g^2\mu_B^2S(S+1)$ per magnetic ion for a free-ion system with the spin-angular momentum of S. The values at $\zeta=0$ are from the susceptibility measured by Webster and Tebble[8] for $1.5T_C$ and the extrapolated one from their measurements up to 500 K by using the Curie-Weiss law for $4T_C$. The dotted line shows the Lorentzian with $\kappa_1=0.22$ Å^{-1}. The solid lines show the results of the spherical model [Eq. (4)] with the exchange parameters listed in Table I and the observed susceptibility data. Since there are no adjustable parameters for the calculation, the agreement between the observed and calculated results is fairly good.

Nevertheless, we should point out that a nontrivial deviation from the theory is seen at high temperatures. The observed susceptibility at $4T_C$ is nearly flat around the $S=2$ free-ion case except near zone center, in good agreement with the observation for the powdered sample by Ziebeck *et al.*,[10] while the theoretical calculation shows a gradual decrease for a wide q range. In Figure 8, the temperature dependence of the inverse of wavelength-dependent susceptibilities is shown. The solid line is the inverse of the observed static susceptibility measured by Webster and Tebble.[8] The dashed-dotted and dashed lines represent values calculated by using Eq. (4) for $\mathbf{q}=(0.08,0.08,0.08)$ and $(0.46,0.46,0.46)$, respectively. Note that the susceptibility at $\mathbf{q}=(0.08,0.08,0.08)$ exhibits

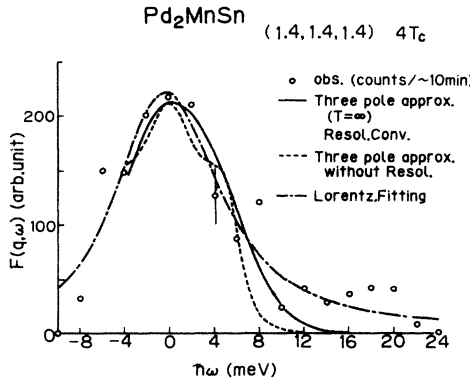

FIG. 6. Comparison between the observed and calculated spectra at $\mathbf{Q}=(1.4,1.4,1.4)$. Open circles are the observed data at $4T_C$. Dashed line is the calculated spectral shape function (TPA, $T=\infty$) without the resolution convolution. Solid line is the calculated spectrum after resolution convolution. Dashed-dotted line is the curve fit to the data by employing the Lorentzian as the spectral shape function.

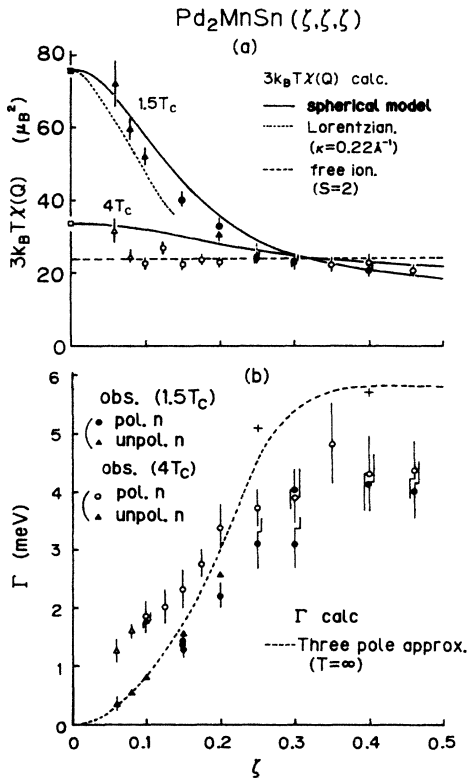

FIG. 7. (a) Wavelength-dependent susceptibility at $1.5T_C$ (solid symbols) and $4T_C$ (open symbols) along [111] direction. Solid and open squares are from the susceptibility data (Ref. 8) at $1.5T_C$ and $4T_C$. Lines are the calculated values. (b) Widths (HWHM) of the spectral shape function at $1.5T_C$ (solid circles and triangles by Lorentzian fit) and at $4T_C$ (open circles and triangles by Lorentzian fit, crosses by Gaussian fit) along [111] direction. Dashed line is the result of three-pole approximation at $T=\infty$.

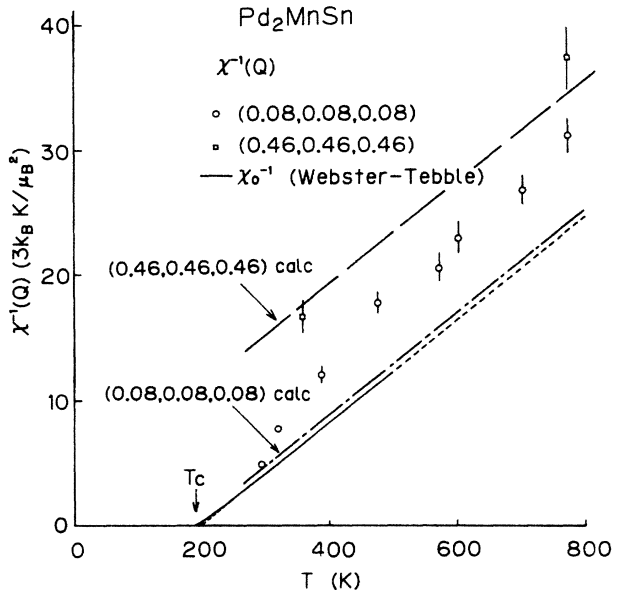

FIG. 8. Temperature dependence of the inverse wavelength-dependent susceptibility at $\mathbf{q}=\mathbf{0}$ [Webster-Tebble (Ref. 8), solid line], $\mathbf{q}=(0.08,0.08,0.08)$ (open circles) and $\mathbf{q}=(0.46,0.46,0.46)$ (open squares). Dashed-dotted and dashed lines are the results of the theory [Eq. (4)].

a clear deviation from the theory for $T \gtrsim 2T_C$, while there is no substantial deviation at $\mathbf{q}=(0.46,0.46,0.46)$.

VI. LINEWIDTH

In Fig. 9 are shown the wave-vector dependence of linewidth [half-width at half maximum (HWHM)] along the [100], [011], and [111] directions determined from the least-squares-fitting procedure to the data at $1.5T_C$ (solid circles) and at $4T_C$ (open circles) by employing the Lorentzian form of the spectral shape function. For the [111] direction, more detailed results are also shown in Fig. 7(b). Since it is difficult to determine the correct spectral shape from the experimental data because of the relaxed resolution and low-counting statistics, the values of the linewidth might contain some uncertainties coming from the choice of the spectral shape function except near the zone center where the Lorentzian becomes the best approximation. In fact, if the Gaussian is assumed to be the spectral shape function instead of the Lorentzian, the least-squares-fitting procedures give larger widths than the case of the Lorentzian; for example, the linewidths at (1.25,1.25,1.25) and (1.4,1.4,1.4,) at $4T_C$ for the Gaussian fit are about 30% larger than those of the Lorentzian case as shown in Fig. 7(b) (crosses). Therefore, in the discussion below, this kind of uncertainty should be taken into account.

The dashed lines in Figs. 7(b) and 9 are the calculated widths at $T=\infty$ by the three-pole approximation based on the Heisenberg model for this system. It is noteworthy that the observed linewidths near the zone boundaries are almost temperature independent and agree well with the calculated values if we take into account the ambiguity discussed above. Note that the agreement between the observed and the calculated widths is much improved if the Gaussian is employed as the spectral shape function instead of the Lorentzian in the fitting procedures. Since the Gaussian form gives nearly the same spectra as the results of the three-pole approximation near the zone boundaries as discussed in Sec. IV, this fact may imply that the main part of the observed spectra near the zone boundaries are determined by the Heisenberg nature in this system.

On the other hand, the observed widths near the zone center are anomalously large compared with the theoreti-

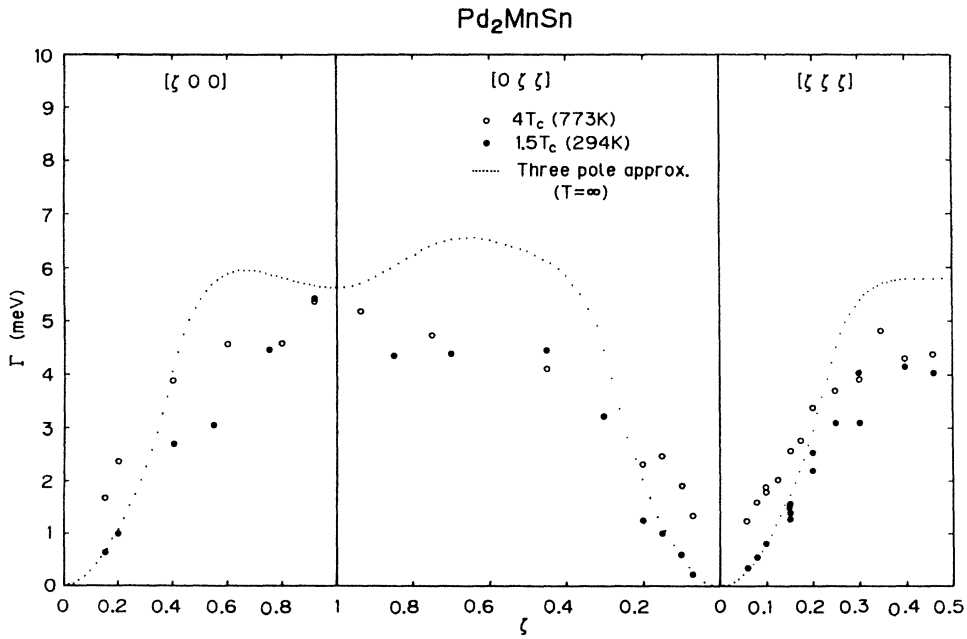

FIG. 9. Linewidths obtained by the Lorentzian fit along [100], [011], and [111] directions at $1.5T_C$ (solid symbols) and $4T_C$ (open symbols). Dashed lines are the calculated by three-pole approximation at $T=\infty$.

cal values. This phenomenon is especially remarkable for the data at $4T_C$, where the linewidths near the zone center are quite large and show no q^2 dependence at least for $q \gtrsim 0.1$ Å^{-1} as shown in Figs. 7(b) and 9. This point is hardly understood by the spin-diffusion picture which is generally accepted for the Heisenberg paramagnet at high temperatures. It is noted that the anomalously large widths are observed at $4T_C$ in the wave-vector region where the $\chi(q)$ deviates substantially from the calculation based on the Heisenberg model as seen in Figs. 7(a) and 7(b).

In Fig. 10, the observed linewidths at $\mathbf{Q}=(1.08,1.08,1.08)$ are shown as the function of T_C/T (open circles). The data below room temperature (solid circles) are from Shirane *et al.*[11] The calculated result by the three-pole approximation at $T=\infty$ for the Pd_2MnSn structure using the exchange parameters up to the sixth-nearest neighbor is indicated by a solid square. The solid line is the calculated results using the spin-diffusion constant given by Hubbard[14] for the case of the simple-cubic nearest-neighbor Heisenberg interaction system with the exchange interaction value of $J=0.62$ meV, which gives the same spin-wave stiffness constant as the observed value of Pd_2MnSn at low temperature. At $T=\infty$, Hubbard's result agrees well with the calculation by the three-pole approximation for the same case (open square), and is about 50% greater than that for the long-range interaction case. Therefore, it is reasonable to consider that, at finite temperatures, the three-pole approximation for the Pd_2MnSn structure would give a somewhat lower value than the solid line in the figure. The dashed curve is calculated by the Résibois-Piette function[23] using the inverse correlation length determined by Shirane *et al.*[11] The discrepancy between the observed linewidth and the estimation by the Heisenberg model is remarkable.

These facts are in contrast with the case of the insulating ferromagnet EuO, where the agreement between the observation and the calculations based on the Heisenberg model is good within the hydrodynamic regime up to

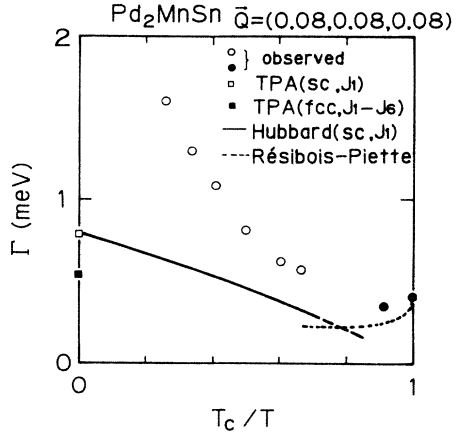

FIG. 10. Temperature dependence of the linewidth at $\mathbf{Q}=(1.08,1.08,1.08)$. Solid line is from the Hubbard calculation for simple-cubic nearest-neighbor interaction case (scNN). Results of three-pole approximation are open square (scNN) and solid square (Pd_2MnSn case). Dashed line is Résibois-Piette function.

$2T_C$.[16,17] Recently, Böni and Shirane[13] found for EuO that, at T_C, the three-pole approximation gives too small linewidths near the zone center than the observed values. However, it is not the case at high temperatures since the three-pole approximation gives the spin-diffusion coefficient which agrees with the observed value[17] as well as those calculated by the other approximations[15] at the high-temperature limit.

VII. DISCUSSION

The present experiment on Pd_2MnSn revealed two important facts for the spin dynamics of the metallic localized spin system. Firstly, the main feature of the scattering function $S(q,\omega)$ at high temperatures is explained well, even quantitatively at least near the zone boundaries, by the theories based on the Heisenberg model with the long-range interaction. This indicates strongly that the Heisenberg-type interactions between localized spins play a major role on the spin dynamics in this system. In other words, the present work confirms the commonly accepted localized spin picture for this material from the viewpoint of the spin dynamics at high temperatures.

As for the spectral shape, no spin-wave-like mode was observed over the entire q and temperature of the measurements. It is not clear at present whether the small shoulder at the finite energy which is expected by the three-pole approximation exists or not near the zone boundaries. We intend to clarify this point experimentally in the near future.

Second, the nontrivial deviations from the theory based on the Heisenberg model were observed in the $\chi(q)$ and linewidth at small q at high temperatures. There exists anomalous damping of the long-wavelength fluctuations of localized spins in this alloy at high temperatures. It may weaken the spatial correlation of the localized spins, and this is compatible with the observed flat $\chi(q)$ at $4T_C$. The long tails of the spectra for $\hbar\omega \gtrsim 10$ meV which cannot be explained by the Heisenberg model might also be related to the effects.

Since our system is metallic and the localized spins on manganese atoms interact with conduction electrons, it is very likely to ascribe the origin of the anomalies to the nonadiabatic effects of conduction electrons on the localized spins. The simplest and commonly accepted picture for our system is the *s-d* exchange interaction model. In fact, this model is convenient to explain the experimental result for the spin dynamics described above because the second-order perturbation theory gives the Heisenberg-type effective interactions between localized spins under the adiabatic approximation for the motion of the localized spins.[24–26] However, since the adiabatic approximation cannot always be allowed in this model,[27] some deviations of spin dynamics from that of the pure Heisenberg interaction system can be naturally expected. The nonadiabatic effect in the ferromagnetic case has been demonstrated theoretically by Nagaoka.[28] The main results of his work is that the dispersion of the adiabatic spin-wave mode is greatly modified near the edges of the Stoner continuum of the conduction electrons and that inside the continuum there arises additional damping of spin waves.

The effects in the paramagnetic case have not yet been calculated theoretically. However, we can speculate on the effects in analogy with the ferromagnetic case as follows. The first point to be mentioned is the increase of the linewidth of the spin fluctuations. This is because each mode of localized spin fluctuation via conduction electrons may suffer from some additional damping effects through spin-flip excitations in the conduction band with the same frequency and momentum transfer as those of the mode. This effect must be prominent in small momentum transfer region for the paramagnetic state because only electrons near the Fermi surface can contribute to this effect. Second, the nonadiabatic effect should become important at high temperatures. This is because the smearing of the Fermi surface occurs nearly in proportion to $k_B T$ and it increases the transition probability of the spin-flip excitations with small momentum and energy transfer in the conduction-electron band. These features are compatible with the observed anomalies described above.

The nearly same phenomena were observed for the spin dynamics of a metallic antiferromagnet Pt_3Fe.[29] Such effects would also be expected for the spin dynamics of the itinerant ferromagnets Fe and Ni since $3d$ itinerant electrons directly contribute to the formation of atomic local moments in these materials. We hope that our conjecture would promote further discussion on this effect from both theoretical and experimental sides.

ACKNOWLEDGMENTS

The authors would like to thank P. Böni and O. Sakai for stimulating discussions. This work was carried out as part of Japan—U.S. Cooperative Neutron Scattering program. One of the authors (M.K.) would like to thank the members of the Brookhaven Neutron Scattering Group for their hospitality during his stay there. The work at Brookhaven National Laboratory was supported by the Division of Materials Sciences, U.S. Department of Energy under Contract No. DE-AC02-76CH00016.

---

*Y. Ishikawa died on 28 February 1986.

†Present address: Institute for Solid State Physics, University of Tokyo, Minatoku, Tokyo 106, Japan.

[1]J. W. Lynn, Phys. Rev. B **11**, 2624 (1975).

[2]J. W. Lynn and H. A. Mook, Phys. Rev. B **23**, 198 (1981).

[3]J. P. Wicksted, P. Böni, and G. Shirane, Phys. Rev. B **30**, 3655 (1984).

[4]P. Böni and G. Shirane, J. Appl. Phys. **57**, 3012 (1985).

[5]H. A. Mook and J. W. Lynn, J. Appl. Phys. **57**, 3006 (1985).

[6]J. W. Lynn and H. A. Mook, J. Magn. Magn. Mater. **54-57**, 1169 (1986).

[7]J. L. Martínez, P. Böni, and G. Shirane, Phys. Rev. B **32**, 7032 (1985).

[8]P. J. Webster and R. S. Tebble, J. Appl. Phys. **39**, 471 (1976).

[9]Y. Noda and Y. Ishikawa, J. Phys. Soc. Jpn. **40**, 690 (1976).

[10]K. R. A. Ziebeck, P. J. Webster, P. J. Brown, and J. A. C. Bland, J. Magn. Magn. Mater. **24**, 258 (1981).

[11]G. Shirane, Y. J. Uemura, J. P. Wicksted, Y. Endoh, and Y. Ishikawa, Phys. Rev. B **31**, 1227 (1985).

[12]H. A. Mook, Phys. Rev. Lett. **46**, 508 (1981).

[13]P. Böni and G. Shirane, Phys. Rev. B **33**, 3012 (1986).

[14]J. Hubbard, J. Phys. C **4**, 53 (1971).

[15]S. W. Lovesey and R. A. Meserve, J. Phys. C **6**, 79 (1971).

[16]P. A. Lindgård, Phys. Rev. B **27**, 2980 (1983).

[17]O. W. Dietrich, J. Als Nielsen, and L. Passel, Phys. Rev. B **14**, 4923 (1976).

[18]H. G. Bohn, A. Kollmar, and W. Zinn, Phys. Rev. B **30**, 6504 (1984).

[19]W. Marshall and R. D. Lowde, Rep. Prog. Phys. **31**, 705 (1968).

[20]M. Takahashi, J. Phys. Soc. Jpn. **52**, 3592 (1983).

[21]A. P. Young and B. S. Shastry, J. Phys. C **15**, 4547 (1982).

[22]M. F. Collins and W. Marshall, Proc. Phys. Soc. London **92**, 390 (1967).

[23]P. Résibois and C. Piette, Phys. Rev. Lett. **24**, 514 (1970).

[24]M. R. A. Ruderman and C. Kittel, Phys. Rev. **96**, 99 (1954).

[25]T. Kasuya, Prog. Theor. Phys. **16**, 45 (1956).

[26]K. Yoshida, Phys. Rev. **106**, 893 (1957).

[27]H. Hasegawa, Prog. Theor. Phys. **21**, 483 (1957).

[28]Y. Nagaoka, Prog. Theor. Phys. **28**, 1033 (1962).

[29]M. Kohgi and Y. Ishikawa, J. Phys. Soc. Jpn. **49**, 985 (1980); **49**, 994 (1980).